

Molecularly Imprinted Polymers: Paving the Way for Future Drug Delivery Innovations

Roongnapa Suedee*, Watchara Pholsathien, Kanok-on Jaisawan, Jittiya Rodruksa, Pistawus Khomintr

Department of Pharmaceutical Chemistry, Prince of Songkla University, Hatyai, Songkhla, Thailand

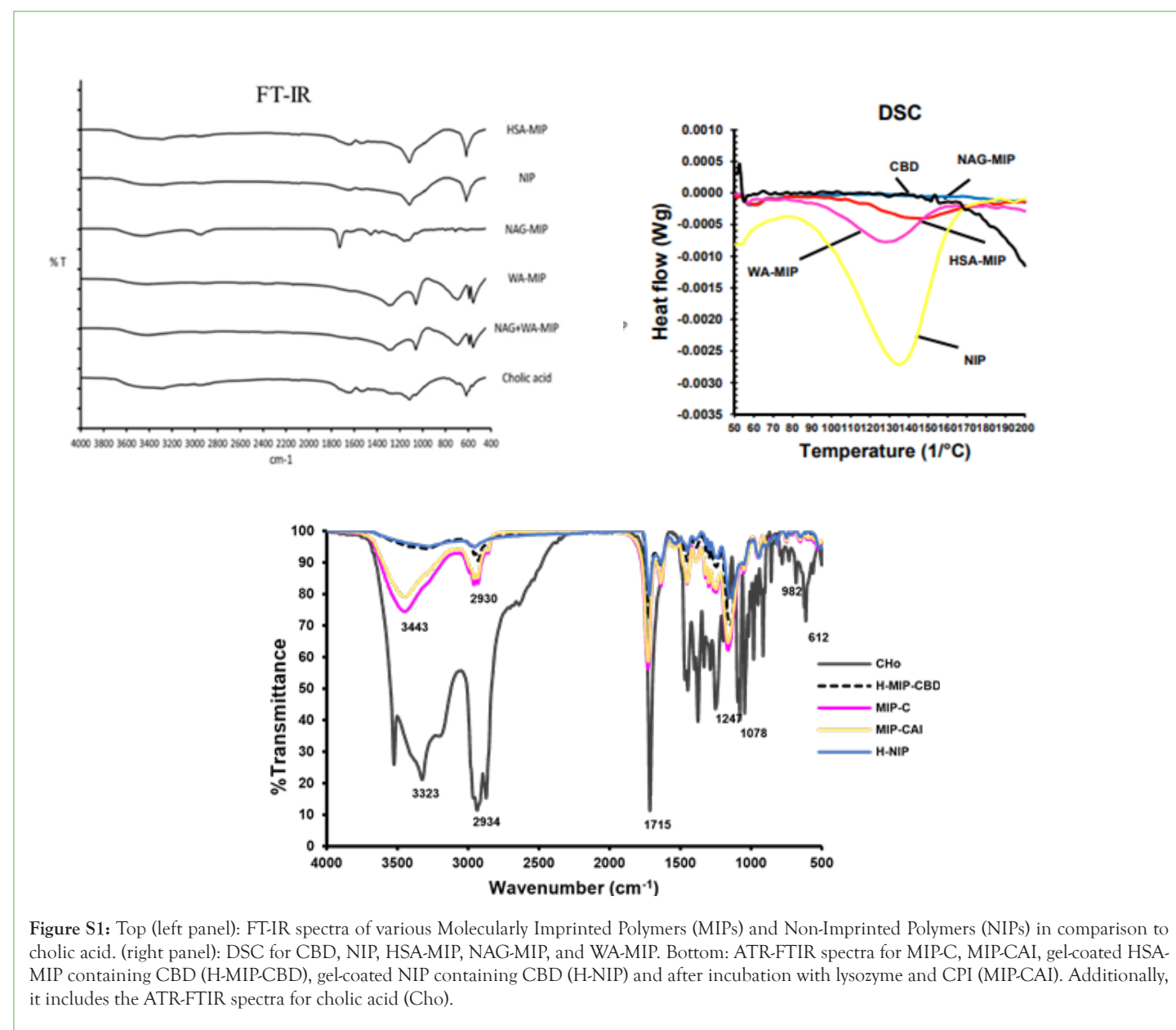


Figure S1: Top (left panel): FT-IR spectra of various Molecularly Imprinted Polymers (MIPs) and Non-Imprinted Polymers (NIPs) in comparison to cholic acid. (right panel): DSC for CBD, NIP, HSA-MIP, NAG-MIP, and WA-MIP. Bottom: ATR-FTIR spectra for MIP-C, MIP-CAI, gel-coated HSA-MIP containing CBD (H-MIP-CBD), gel-coated NIP containing CBD (H-NIP) and after incubation with lysozyme and CPI (MIP-CAI). Additionally, it includes the ATR-FTIR spectra for cholic acid (Cho).

Correspondence to: Roongnapa Suedee, Department of Pharmaceutical Chemistry, Prince of Songkla University, Hatyai, Songkhla, Thailand, E-mail: roongnapa.s@psu.ac.th

Received: 19-Jul-2025, Manuscript No. PAA-25-29459; **Editor assigned:** 22-Jul-2025, PreQC No. PAA-25-29459 (PQ); **Reviewed:** 05-Aug-2025, QC No. PAA-25-29459; **Revised:** 11-Aug-2025, Manuscript No. PAA-25-29459 (R); **Published:** 19-Aug-2025, DOI: 10.4172/2153-2435.25.16.822

Citation: Suedee R, Pholsathien W, Jaisawan K, Rodruksa J, Khomintr P (2025). Molecularly Imprinted Polymers: Paving the Way for Future Drug Delivery Innovations. Pharm Anal Acta. 16:822.

Copyright: © 2025 Suedee R, et al. This is an open-access article distributed under the terms of the Creative Commons Attribution License, which permits unrestricted use, distribution, and reproduction in any medium, provided the original author and source are credited.

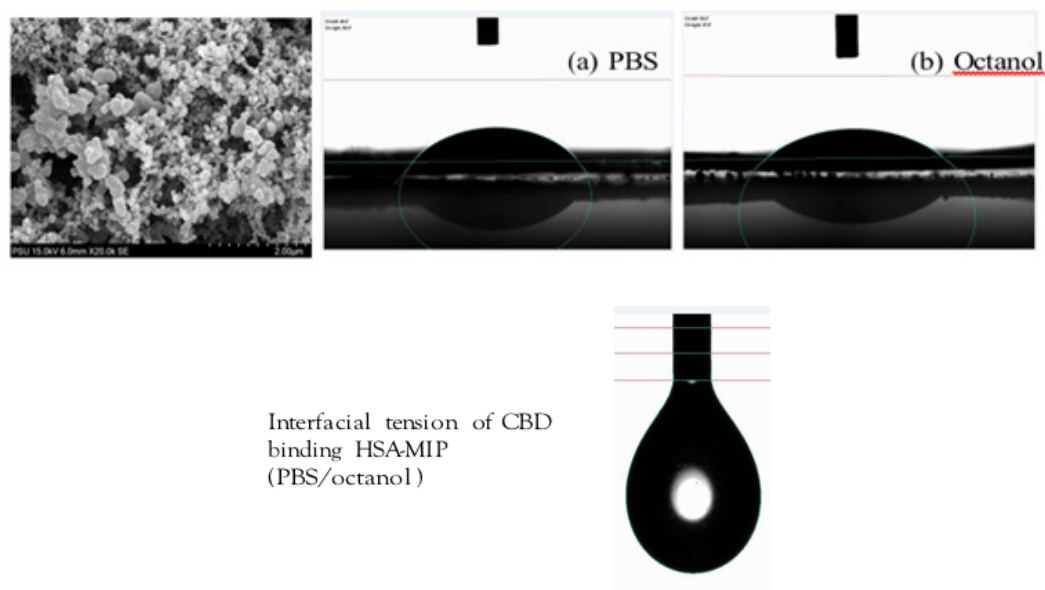


Figure S2: (A) left panel: SEM image of the drop-coated human serum albumin molecularly imprinted polymer (HSA-MIP) containing Cannabidiol (CBD), referred as MIP-C. The contact angle of HSA-MIP is assessed in both phosphate-buffered saline (PBS) and octanol.

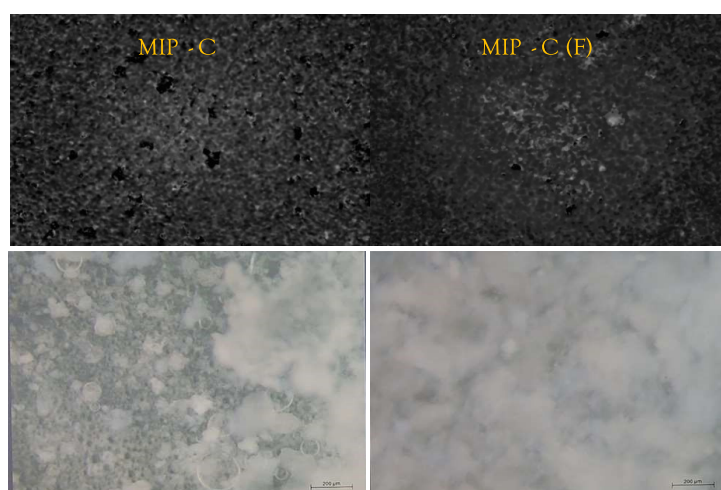


Figure S3: Bright field image of MIP-C before and after adding the excipients in drug formulation, MIP-C (F).

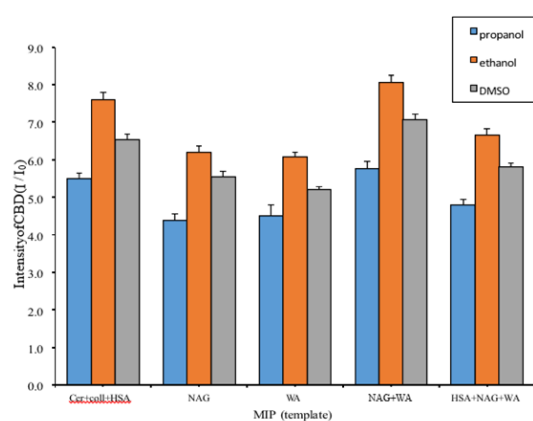


Figure S4: The intensity of CBD (I/I_0) in various solvents was assessed in relation to a single or a mixture of Molecularly Imprinted Polymers (MIPs) prepared using Nacetylglucosamine (NAG), Wheat Germ Agglutinin (WGA), and Human Serum Albumin (HSA) as templates, conducted at room temperature.

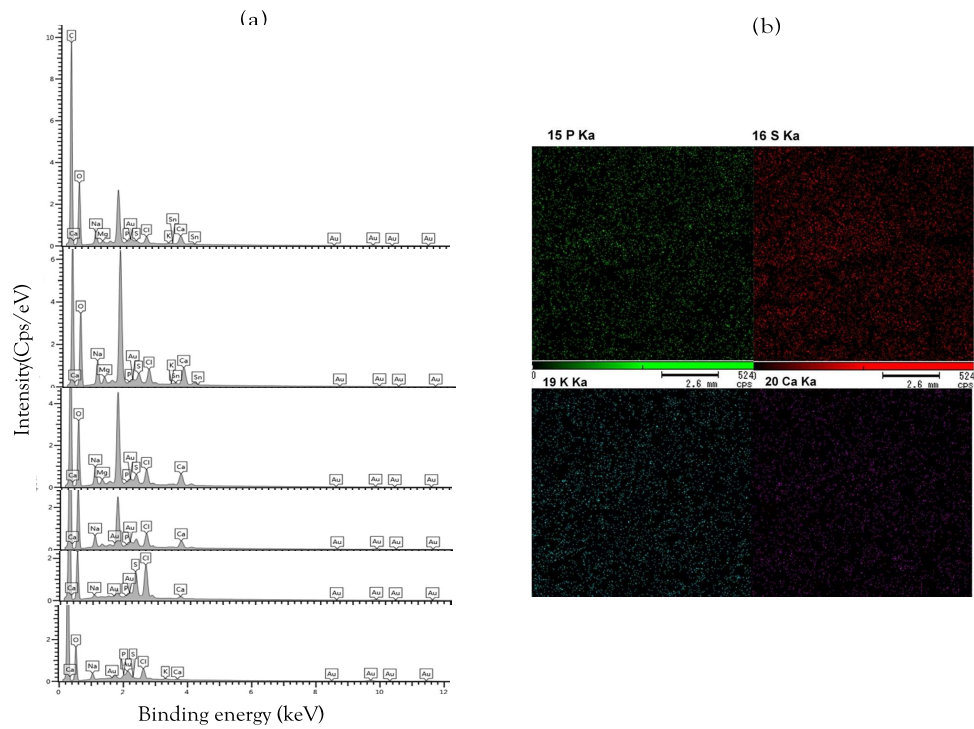


Figure S5: (a) A qualitative profile of map sum spectrum for the effect of the incubation of lysozyme and CPI on high CBD loading in HM-CAI under the octanol/ PBS solution, and (b) Right panel: XRF mapped images showing atomic molecules localized within the EPS cellulose membrane.

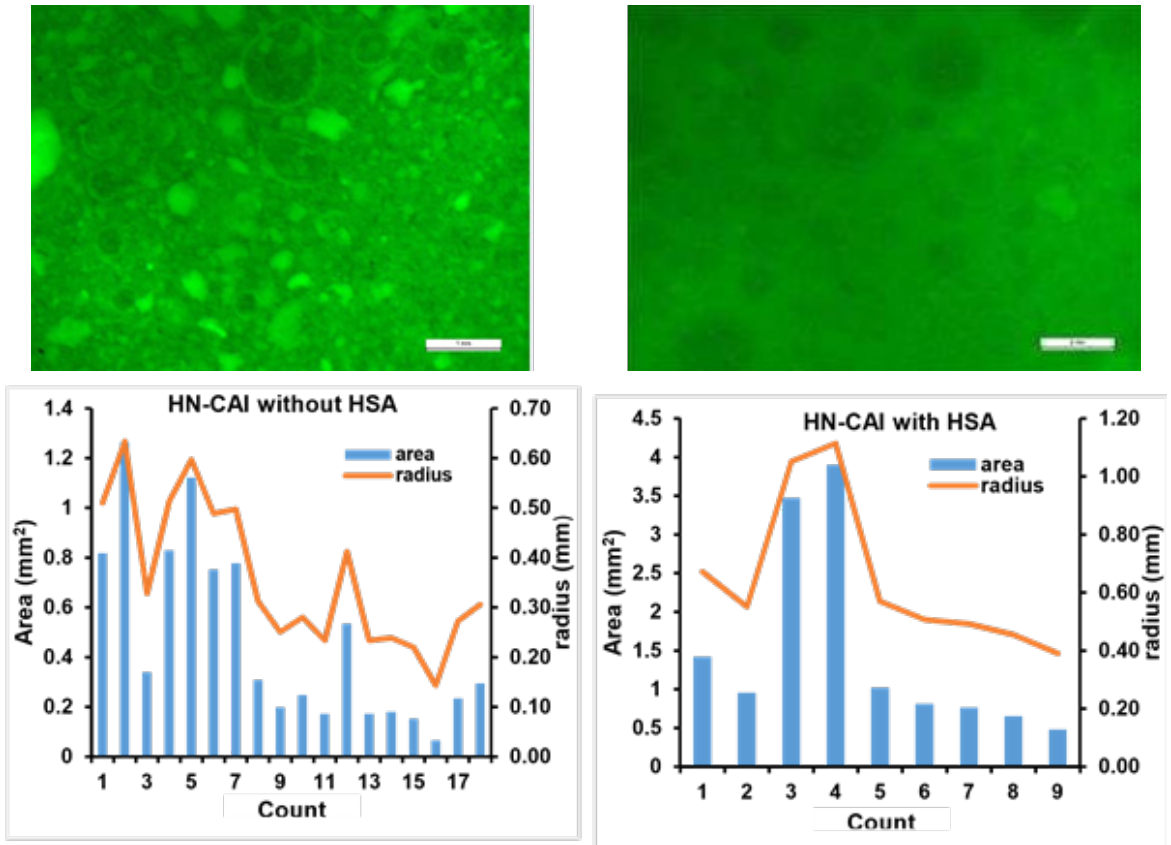


Figure S6: The captivating images and plot showing the relationship between area (mm²) and radius for subvisible aggregated particles from HN-CAI samples, before and after adding HSA.

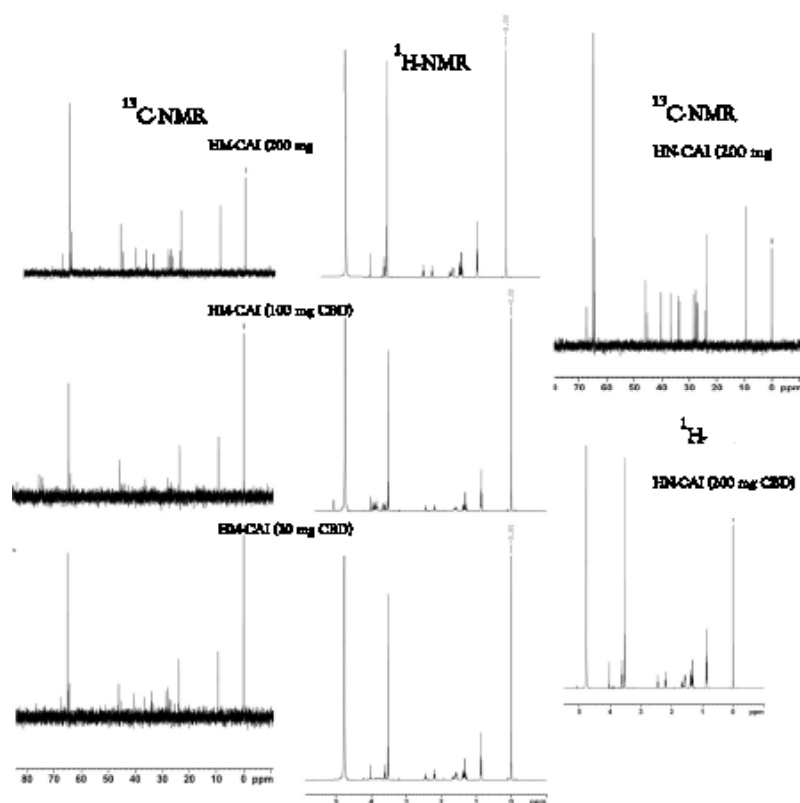


Figure S7: The effect of CBD loading on ^1H -NMR and ^{13}C -NMR for MIPs and NIP nanocapsules from the filtered reservoirs and the excipient-rich phase demonstrates a spatial disturbance and change in protein volume.

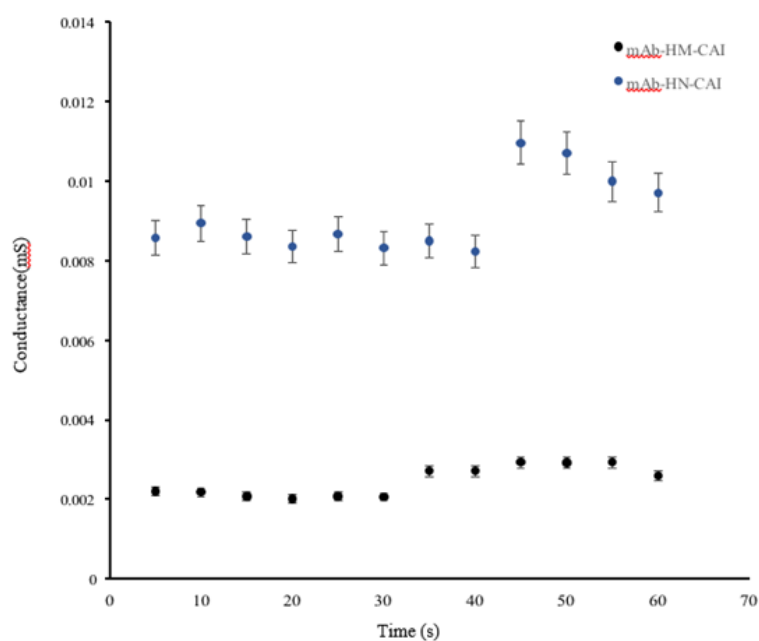


Figure S8: Illustrates the conductivity changes in the protein and CBD-loaded nanocapsules for the MIP and NIP derived from the filtered reservoir.

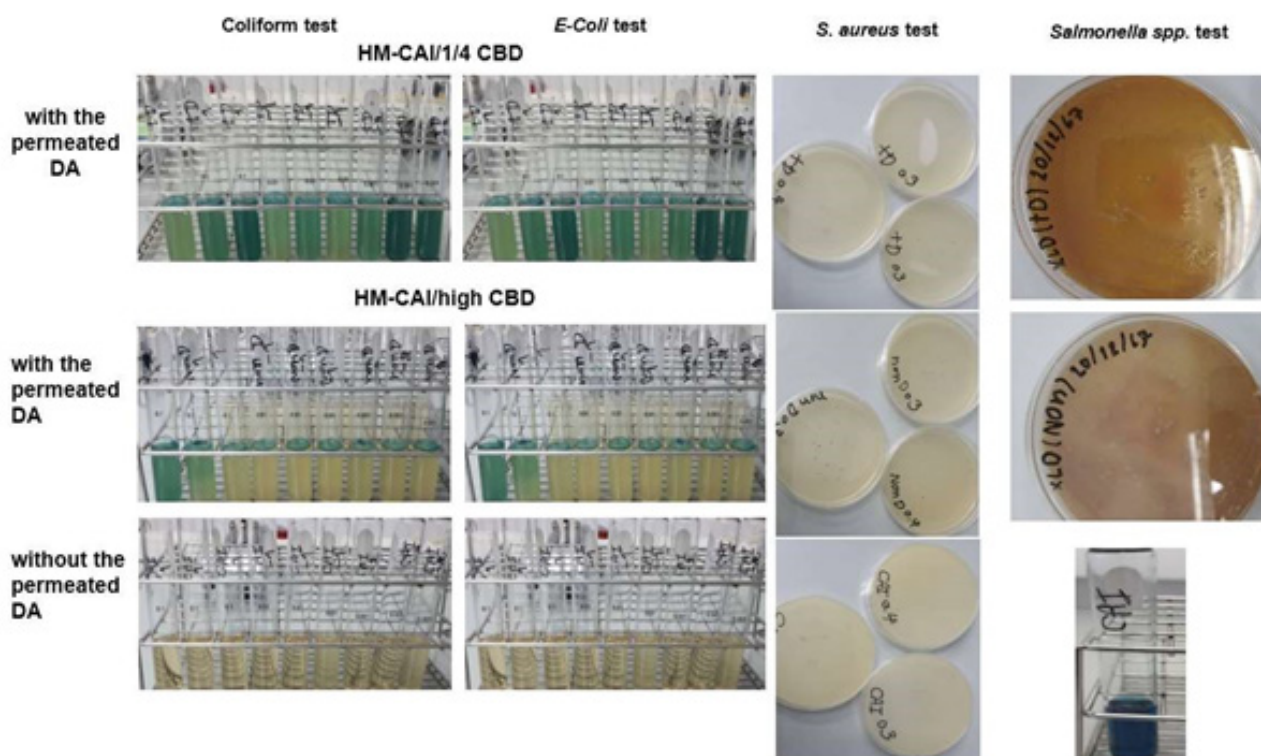


Figure S9: The determination of the presence of Coliform, *Staphylococcus aureus*, *Escherichia coli*, and *Salmonella* species in samples. The method employed for detecting the growth of these microorganisms or their metabolic products involves colour change in LMS broth, which precedes the thorough strain typing on XLD agar plates. Colony counts of a series of filtered liquid samples. According to the british pharmacopoeia 2023, when we used a special filtering method on the water, and diluted the samples.

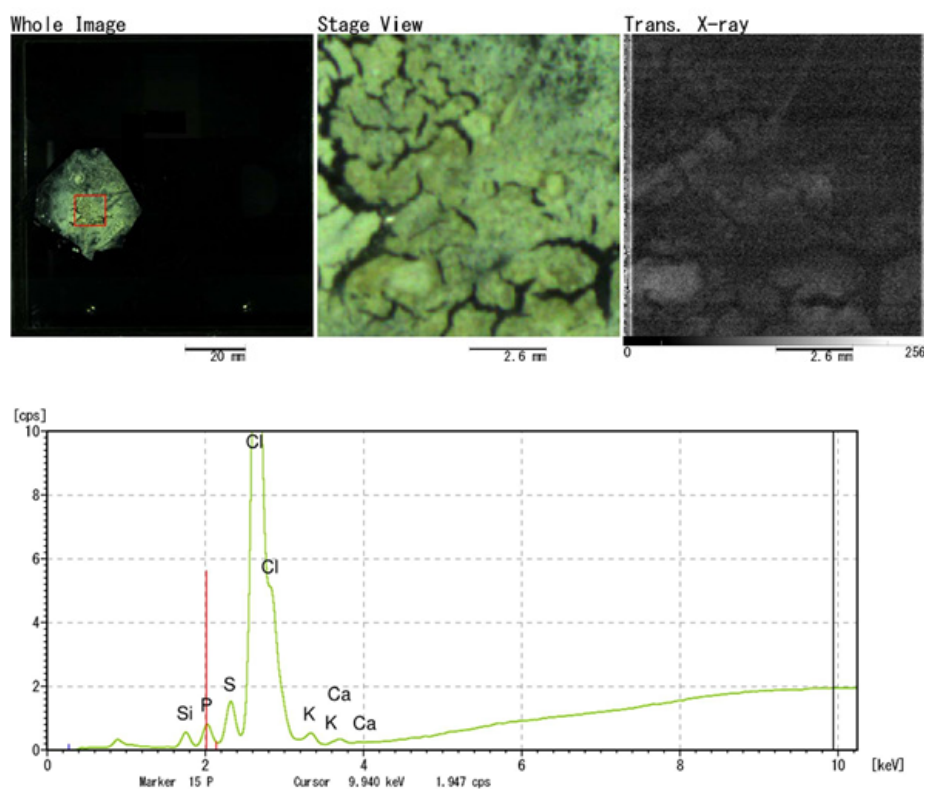


Figure S10: Fluorescence intensities (keV) of the biocompositions, the filtered nanocapsules, and HM-CAI remained at the cellulose/PBS interface.

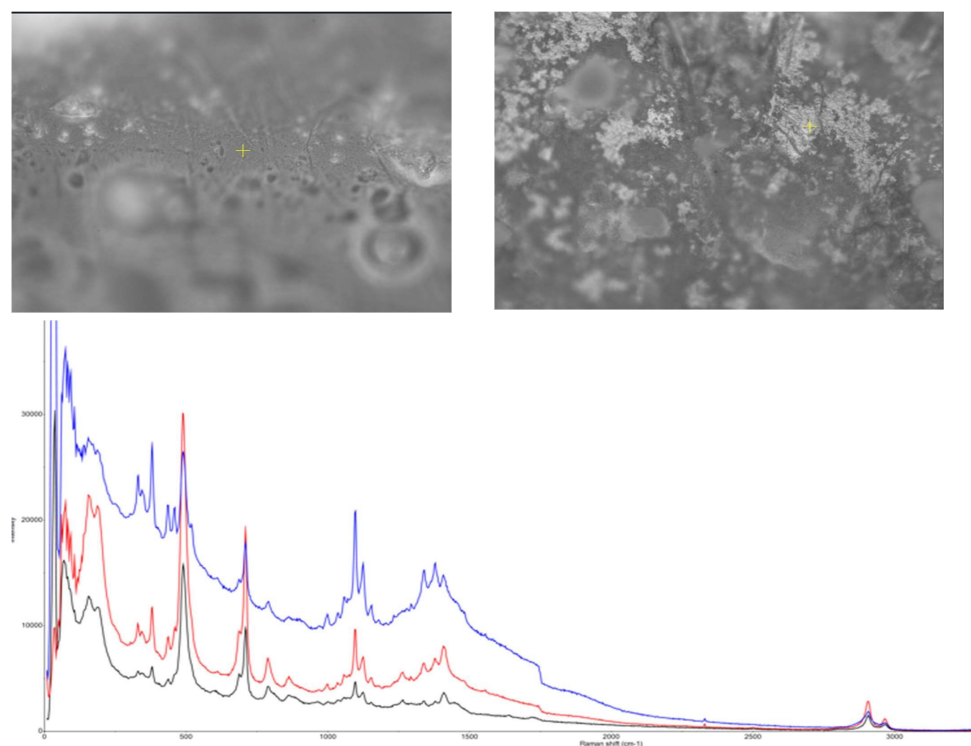


Figure S11: (a) Channel hydrates of the biocompositions dried on the cellulose/PBS interface and (b) the solubility of CBD, along with combined mAb and insulin in sink dissolution and diffusion. Below: Raman mapping spectra from three locations on or near the dried droplet of a filtered reservoir HN-CAI.

Table S1: Microbial test at 0.1, 0.01, and 0.001 g inocula, the MPNs per gram and 95 percent confidence intervals. N=3

| Pos. tubes | | | MPN/g | Conf. lim. | | Pos. tubes | | | MPN/g | Conf. lim. | |
|------------|--------|--------|-------|------------|------|------------|-------|--------|-------|------------|------|
| 0.1 g | 0.01 g | 0.001g | | Low | High | 0.1g | 0.01g | 0.001g | | Low | High |
| 0 | 0 | 0 | <3.0 | ~ | 9.5 | 2 | 2 | 0 | 21 | 4.5 | 42 |
| 0 | 0 | 1 | 3 | 0.15 | 9.6 | 2 | 2 | 1 | 28 | 8.7 | 94 |
| 0 | 1 | 0 | 3 | 0.15 | 11 | 2 | 2 | 2 | 35 | 8.7 | 94 |
| 0 | 1 | 1 | 6.1 | 1.2 | 18 | 2 | 3 | 0 | 29 | 8.7 | 94 |
| 0 | 2 | 0 | 6.2 | 1.2 | 18 | 2 | 3 | 1 | 36 | 8.7 | 94 |
| 0 | 3 | 0 | 9.4 | 3.6 | 38 | 3 | 0 | 0 | 23 | 4.6 | 94 |
| 1 | 0 | 0 | 3.6 | 0.17 | 18 | 3 | 0 | 1 | 38 | 8.7 | 110 |
| 1 | 0 | 1 | 7.2 | 1.3 | 18 | 3 | 0 | 2 | 64 | 17 | 180 |
| 1 | 0 | 2 | 11 | 3.6 | 38 | 3 | 1 | 0 | 43 | 9 | 180 |
| 1 | 1 | 0 | 7.4 | 1.3 | 20 | 3 | 1 | 1 | 75 | 17 | 200 |
| 1 | 1 | 1 | 11 | 3.6 | 38 | 3 | 1 | 2 | 120 | 37 | 420 |
| 1 | 2 | 0 | 11 | 3.6 | 42 | 3 | 1 | 3 | 160 | 40 | 420 |
| 1 | 2 | 1 | 15 | 4.5 | 42 | 3 | 2 | 0 | 93 | 18 | 420 |
| 1 | 3 | 0 | 16 | 4.5 | 42 | 3 | 2 | 1 | 150 | 37 | 420 |

| | | | | | | | | | | | |
|---|---|---|-----|-----|----|---|---|---|-------|-----|-------|
| 2 | 0 | 0 | 9.2 | 1.4 | 38 | 3 | 2 | 2 | 210 | 40 | 430 |
| 2 | 0 | 1 | 14 | 3.6 | 42 | 3 | 2 | 3 | 290 | 90 | 1,000 |
| 2 | 0 | 2 | 20 | 4.5 | 42 | 3 | 3 | 0 | 240 | 42 | 1,000 |
| 2 | 1 | 0 | 15 | 3.7 | 42 | 3 | 3 | 1 | 460 | 90 | 2,000 |
| 2 | 1 | 1 | 20 | 4.5 | 42 | 3 | 3 | 2 | 1100 | 180 | 4,100 |
| 2 | 1 | 2 | 27 | 8.7 | 94 | 3 | 3 | 3 | >1100 | 420 | - |